Indian Journal of Pure & Applied Physics
Vol. 61, May 2023, pp. 326-334
DOI: 10.56042/ijpap.v61i5.70933

Influence of pH on the Properties of Chemically Prepared SnS and CdS Thin Films

Smiya John[a,b]*, Melda Francis[b], Reena Mary A P[a] & V Geetha[a]

[a]Department of Physics, Govt.Victoria College (affiliated to University of Calicut) Palakkad Kerala 678 001, India
[b]Department of Physics, Mercy College (affiliated to University of Calicut) Palakkad Kerala 678 006, India

Received 28 January 2023; accepted 10 April 2023

The SnS and CdS thin films were chemically prepared from the bath solutions with different pH values of 9.8, 9.9, and 10, and 11.3, 11.4, and 11.5 respectively. The X-ray diffraction confirmed the formation of orthorhombic SnS with a preferred orientation along the 013 plane and cubic CdS along the 311 planes. Crystallite size and lattice strain were calculated from the Williamson-Hall plot, and it was found that the crystallite size increased as pH increased. Raman spectra showed the prominent peaks of SnS and CdS thin films. Optical studies revealed a decrease in the optical band gap of both samples with increasing pH values. SnS films showed needle-like morphology with agglomerates and CdS flake-like interconnected structures. From the EDS analysis, it was noticed that both the SnS and CdS thin films shifted to a metal-rich composition with the increase in the pH of the bath solution. Finally, a solar cell (ITO/SnS/CdS/Ag) was made, and it was found that cell structures formed with SnS and CdS that were deposited with pH values of 10 and 11.3 showed better performance.

Keywords: SnS; CdS; XRD measurements; Raman analysis; EDS spectra

1 Introduction

One of the most promising and environmentally friendly energy sources, solar energy, is the subject of extensive research. Due to their low manufacturing costs, high-throughput processing techniques, and ease of junction formation, thin film-based solar cells offer a wide range of applications[1].As a potential absorber material for solar cells, orthorhombic tin monosulfide (SnS), which is abundant on earth and has ideal electronic properties such as an ideal band gap (~1.3 eV), a high optical absorption coefficient of 10^4 cm^{-1}, and intrinsic p-type conductivity, has attracted a lot of interest[2–4]. Charge transmission between SnS thin layers is supposedly resistant to flaws and impurities, unlike in silicon, which needs high purity and crystal perfection to generate efficient but expensive solar cells. Even in the presence of oxygen and moisture in the atmosphere, SnS is stable. As a result, SnS has a better chance of remaining stable over time than organic solar cells and perovskites, which are damaged by oxygen and moisture. Furthermore, SnS is non-toxic[5]. Theoretical studies by Loferski[6]and simulations by Abdul Kuddus et al.[7]showed that SnS-based solar cells are capable of a sunlight conversion efficiency of more than 20%[8].It thus represents a potential option for use as an absorber layer in a thin-film solar cell. However, the reported power conversion efficiency (η) of SnS-based solar cells remained below 4%[4]. There have been numerous attempts to increase the effectiveness of SnS solar cells. The presence of an indirect band gap and the layered crystal structure of the SnS thin film are also limitations[9]. The main challenges to improving the efficiency of SnS-based solar cells are the production of high-quality SnS thin films and selecting the appropriate n-type semiconductor[10]. Boubakri *et al.*[11] simulated SnS-based solar cell and studied the effect of the quality of the window and buffer layers on the performance of the solar cell. For the window layers of solar cells, semiconductors having band gaps matching the longest wavelength in the visible spectrum are suitable[4]. The CdS, an n type semiconductor with a bulk band gap of 2.42 eV, is a promising window layer material used in both commercial modules and lab research[1,12,13].

Vacuum evaporation[14,15], sputtering[16,17], CVD[18,19], electrodeposition[20,21], pulsed-laser deposition[22,23], spray pyrolysis[24,25], SILAR[26,27], and chemical bath deposition (CBD)[8,28]are some of the techniques used for the deposition of SnS and CdS thin films. CBD is one of the most widely used synthesis routes for the production of inorganic metal chalcogenide and oxide semiconductor thin films due to its many advantages, including large area deposition, relatively low temperature processes, repeatability, and most importantly, low equipment cost.

*Corresponding author: (E-mail: smiyajohn86@gmail.com)

Numerous writers have claimed that the structural, optical, morphological, and chemical characteristics of the various constituent layers have an impact on the efficiency of thin film solar cells [29]. Various factors can be varied to optimize the properties of SnS and CdS thin films,which includes the annealing temperature[26,30–32], bath composition[1,33], deposition time[3,34] and pH of the bath solution[8,20,35]. Nasr et al.[36] proposed that the physical properties of the ZnS thin film can be modified by pH, and V. S. Raut etal.[35]investigated the impact ofthe pH of the bath solution on the structural, optical, and morphological properties of CdSe thin films.In this work, SnS and CdS thin films were prepared chemically, and the influence of pH on their properties was investigated. SnS/CdS heterojunctions were fabricated by taking different combinations of films. The performance of the cells was also evaluated.

2 Experimental Details

2.1 Preparation of SnS Thin Films

In this work, stannous chloride ($SnCl_2.2H_2O$) and thioacetamide (CH_3CSNH_2) were used as tin and sulphur precursors, respectively, to prepare SnS thin films. As complexing agents, triethanolamine N $(CH_2CH_2OH)_3$ (TEA), and trisodium citrate$Na_3C_6H_5O_7.2H_2O$ (TSC), were used to avoid sudden precipitation. All the chemicals used in this work were of analytical grade and were purchased from Merck. Firstly, 0.3 M $SnCl_2.2H_2O$ dissolved in glacial acetic acid was added to 5 ml of 0.6 M trisodium citrate, which was followed by the sequential addition of 5 ml of TEA and 5 ml of 0.1 M thioacetamide. To adjust the pH of the bath solution, Sp. gr.. 91 pure ammonia solution was added. After the addition of the required amount of ammonia, the final solution was made up to 100 ml by the addition of deionized water, and thoroughly cleaned glass substrates were immersed in it. The clear solution was gradually changed to yellow, which eventually turned chocolate brown. The dark brown SnS thin film was obtained at room temperature. For varying the pH, ammonia solution was added in amounts of 3 ml, 4 ml, and 5 ml, and the pH values obtained were 9.8, 9.9, and 10, respectively. The deposition time decreased considerably with the increase in pH. The film formation was completed within 12 hours, 10 hours, and 9 hours for the pH values of 9.8, 9.9, and 10. It was observed that when the pH of the source solution was below 9.8, film formation did not take place even after 48 hours at room temperature. For solutions with a pH value greater than 10, the chemical reaction took place at a faster rate in the ambient conditions, and the film was not formed. The films that were obtained had a dark brown colour. The films were annealed at 60 °C for 30 minutes, and the characterizations were done.

2.2 Preparation of CdS Thin Films

CdS thin films were prepared from a chemical bath containing 0.1 M cadmium acetate ($(CH3COO)_2$ $Cd.2H_2O$) as a cationic precursor, 0.3 M thiourea (CH_4N_2S) as an anionic precursor, triethanolamine (TEA) as a complexing agent, and ammonia as buffer solution[37].Three different bath solutions with pH values of 11.3, 11.4, and 11.5 were used to make the films. The films were not formed for pH values outside this range at ambient conditions. The deposition times for pH values 11.3, 11.4, and 11.5 were respectively 5 hours, 4 hours, and 2 hours. The prepared CdS thin films were yellow in colour and were homogeneous, smooth, and adherent to the substrate. The samples were annealed at 60 °C for 30 minutes and characterized using various techniques.

2.3 Fabrication of SnS/CdS Heterojunction

The heterojunction was formed on a thoroughly cleaned ITO substrate. Firstly, the SnS thin film was coated and annealed as mentioned before, followed by the deposition of CdS. The whole structure was then annealed at 60 °C for 30 minutes. A thin silver contact was taken on the heterojunction. The junction was fabricated by choosing different thin films of SnS and CdS prepared from varying pH of the source solutions, as mentioned earlier, and the I-V characteristics were studied using a Keithley source meter.

3 Results and Discussion

Structural studies of SnS thin films were performed using the Bruker D8 Advance X-ray diffractometer (Cu Kα source). Raman analysis was done using a Horiba Labram HR Evo Raman spectrometer. The annealed films were optically characterized using an Intek UV-vis spectrophotometer. The wavelength used for the characterization was in the range of 190 nm to 1190 nm. Deuterium was used as the source for UV and Tungsten for visible radiation. The morphology of the films was studied using a field emission scanning electron microscope (FESEM SUPRA 55 VP-4132 Carl Zeiss). Energy dispersive spectra (EDS) were recorded along with FESEM to get a better understanding of the chemical composition.

3.1 Reaction Mechanism

The four processes—the simple ion-ion mechanism, simple hydroxide cluster mechanism, the complicated

ion-by-ion decomposition mechanism, and the complex cluster decomposition mechanism—are active during nucleation and film growth in CBD. Ions diffuse over to the substrate in the initial phase of the straightforward ion-ion reaction. The substrate promotes nucleation by acting as a catalyst. As ions in the solution are absorbed, nucleation expands and new crystals are formed. Crystals come together to form a film that uses Van der Waals forces to bind to one another. Hydroxide colloidal particles diffuse to the substrate and adhere there in a straightforward hydroxide colloidal mechanism. Free ions interact with hydroxide colloidal particles that are attached to the substrate. The free ion displaces the hydroxide as a result of this reaction. The first particles produced by reaction stick together to form an aggregated film. In last two processes, the initial ions diffuse to the substrate to generate heterogen nuclei that develop or exist as complexed nuclei colloids in the solution. In the intricate breakdown procedure, first nucleation is exposed to chemical interactions to create a film. To get a high-quality film from CBD, it is necessary to ensure that the reaction in the solution is realized gradually. Metal ions can form a complex with a legend to stop the solid chemical from precipitating quickly. This reaction suggests that film generation can happen via complex mechanisms in addition to simple ion-by-ion or cluster methods. On the basis of all this knowledge about the procedure, it has been assumed that the mechanism below is effective in the creation of SnS thin films on a substrate[38]:

$$[Sn(TEA)]^{2+}+CH_3CSNH_2+2OH^- \rightarrow SnS+TEA+CH_3CONH_2+H_2O$$

During the initial stages of deposition, Sn^{2+} ions formed bonds with the triethanolamine (TEA) ligand to form Sn $[TEA]^{2+}$. This complex served to prevent the precipitation of undesirable materials like $[Sn(OH)_2]$, and at a later stage, the complex broke down to form bonds with sulphur ions, forming SnS compound. Trisodium citrate (TSC) can be substituted for TEA in a similar calculation[39]. When the pH increases, the $[Sn(TEA)]^{2+}$ complex releases more Sn^{2+} ions. As SnS precipitates more quickly in more basic solutions, this results in speedy SnS deposition with increasing ammoniaconcentrations[8]. The same reaction mechanism is applicable to the formation of Cadmium sulphide[1].

3.2 Structural properties

The X-ray diffraction patterns of the prepared samples of SnS (pH: 9.8, 9.9, and 10), and CdS (pH: 11.3, 11.4, and 11.5) with various pH values were displayed in Figs 1(a) & (b), respectively. In SnS thin films, an intense peak was observed at 2θ value of 31.6°, which corresponds to the diffraction from the (0 1 3) plane, while the other peaks determined at 30.5° and 44.5° were indexed with the (1 1 0) and (0 2 2) planes, respectively. All the peaks were indexed and compared with the standard ICDD data card of SnS (ICDD file no. 001-0984), and the crystal structure was found to be orthorhombic. The intense peak observed for CdS thin films was at 51.9°, associated with the (3 1 1) plane of cubic CdS. The miller planes (1 1 1) and (2 0 0) correspond to the minor peaks at 26.5° and 30.6°, respectively. The peaks from the XRD pattern were indexed using the cubic CdS standard card (ICDD file no. 065-2877). It was found that the intensity of the XRD peaks increased with the pH value of the bath solution for both SnS and CdS films.

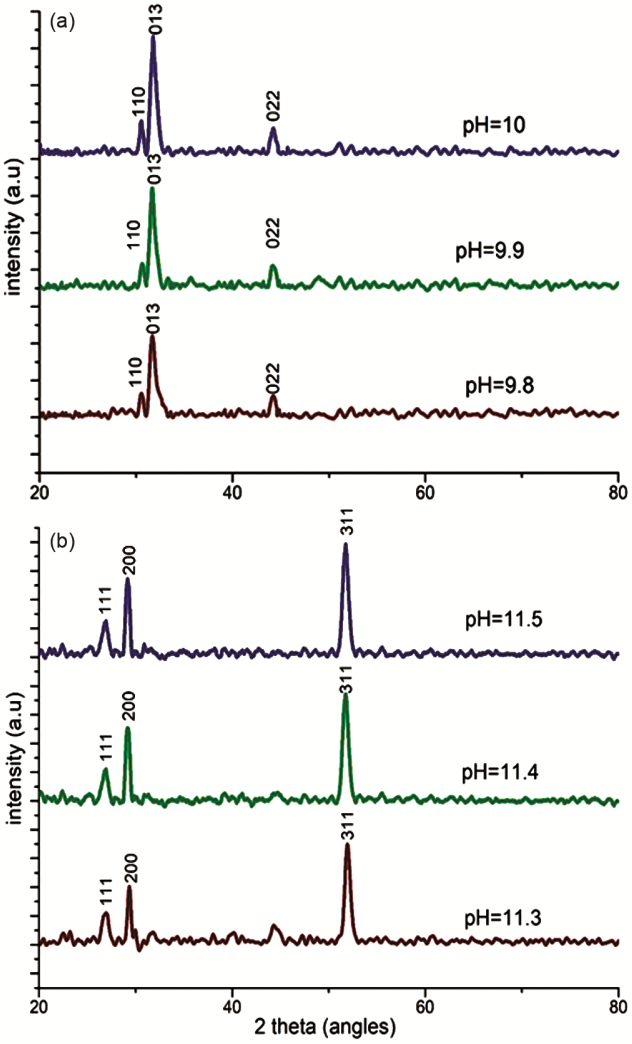

Fig. 1 — X-ray diffraction pattern of (a) SnS and (b) CdS thin films for different pH of the bath solution

3.2.1 Williamson–Hall Method

The Williamson-Hall plots were drawn to determine the crystallite size and strain of the films. The width of the XRD peaks was due to two reasons, one from the crystallite size and the other from lattice strain broadening. The broadening is measured in terms of full width at the half maximum (β).

$$\beta_{total} = \beta_{crystallite\ size} + \beta_{micro\ strain} \quad \ldots (1)$$

The Scherrer equation can be used to calculate the crystallite size broadening while the other uses the strain equation.

$$\beta_{total} = \frac{k\lambda}{D\ cos\theta} + 4\varepsilon\ tan\theta \quad \ldots (2)$$

In the equation (2), k is the shape factor of the value 0.9, λ is the wavelength of the x-ray, which is 1.5406 Å, D is the crystallite size, θ is the Bragg angle, and ε is the micro strain of the lattice. A straight-line equation can be obtained by rearranging this equation.

$$\beta_{total} = \frac{k\lambda}{D\ cos\theta} + 4\varepsilon\ \frac{sin\theta}{cos\theta} \quad \ldots (3)$$

$$\beta_{total} cos\theta\ = \varepsilon\ 4sin\theta + \frac{k\lambda}{D} \quad \ldots (4)$$

Now equation (4) is in the form of the straight-line equation y = mx + c, where m and c are the slope and intercept, respectively. A straight line with microstrain (ε) as the slope and kλ/D as the intercept can be obtained by drawing a graph with 4sinθ on the x-axis and β_{total}cosθ on the y-axis[40,41]. As long as the values of k and λ are known, the crystallite size can be calculated from the intercept.

Figures 2(a-c) & (d-f) show the Williamson-Hall plots of samples prepared from different bath solutions

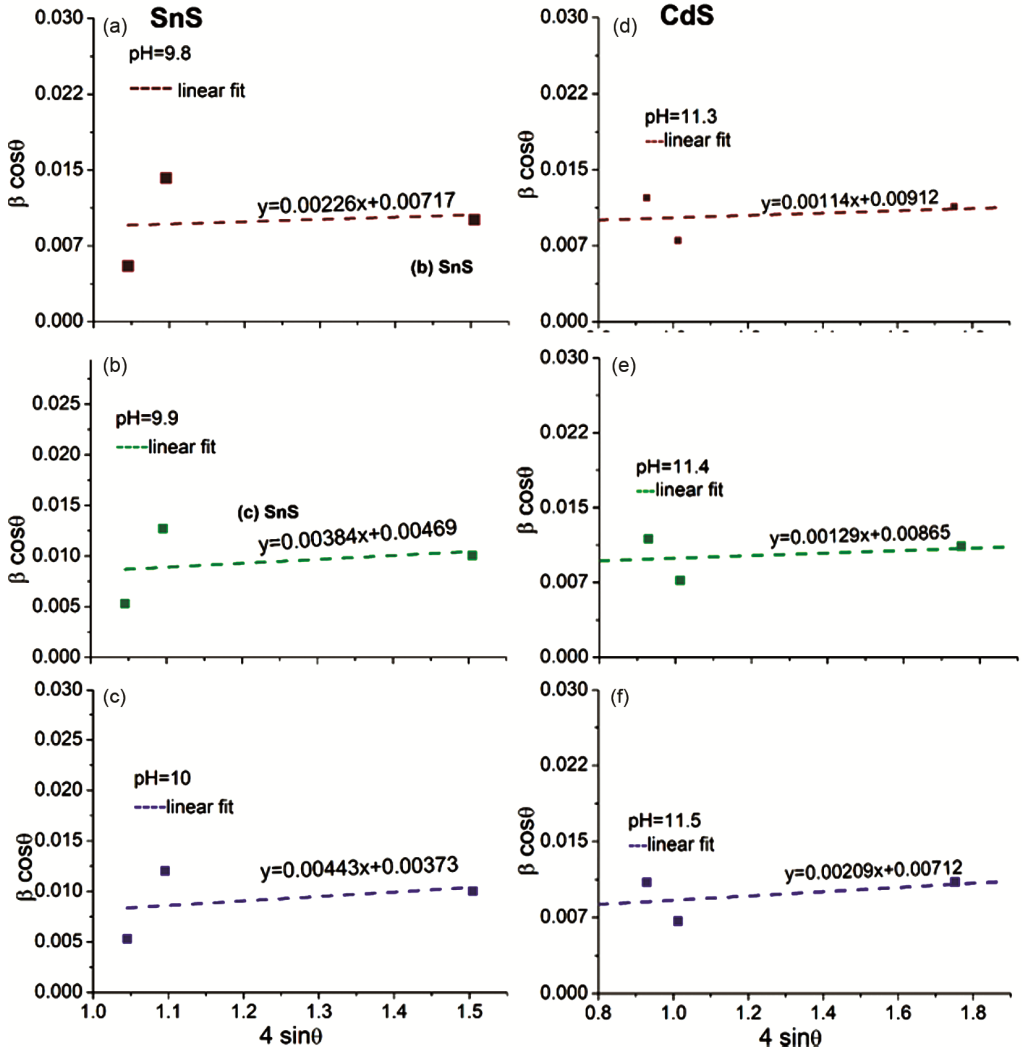

Fig. 2 — Williamson-Hall plots of (a-c) SnS and (d-f) CdS thin films fordifferent pH of the bath solution

with varying pH values for SnS and CdS thin films, respectively. As by equation (4), the microstrain and the crystallite size were obtained from the slope and the intercept of the straight line that was linearly fitted to the obtained points. The crystallite size was found to be 19.3 nm, 33.9 nm, and 37.2 nm for the pH values of 9.8, 9.9, and 10 for SnS thin films, respectively. For CdS thin films, it was found to be 15.2 nm, 16.2 nm, and 19.47 nm for the pH values of 11.3, 11.4, and 11.5. It was observed that as the pH increased, the crystallite size increased, which in turn enhanced crystallinity. Moreover, as pH rises, OH- ions from the ammonia solution increase, which causes more cations to get into the solution, making the thin film more homogeneous and crystalline. The slope of the fitted line gives the micro strain, and it was found to have positive values showing lattice expansion. The internal stress during the formation of the thin film causes a change in the crystallization, and this deformation is termed as microstrain. The microstrain values were 0.00226, 0.00384, and 0.00443 for the pH values of the bath solution, which were 9.8, 9.9, and 10 for SnS thin films, respectively. This is because, as mentioned above, as pH increases, more tin ions get into the solution and make the film denser, which is consistent with the FESEM images. This increase in density increases the strain in the lattice. For the CdS thin films, it was found to be 0.00114, 0.00129, and 0.00209 for the pH values of 11.3, 11.4, and 11.5. The microstrain increases as the pH of the solution increases because more cations in the solution increase the density of the thin films, which causes an increase in the strain.

3.3 Raman Analysis

The Raman spectra of SnS and CdS thin films are shown in Figs 3(a) & (b), respectively. The prominent peaks related to SnS phonon modes are clearly observed at 94 cm^{-1} (A_g), 160 cm^{-1} (B_{2g}), and 221 cm^{-1} (A_g) in the spectra. The B_{2g} mode represents the interaction through the interlayer b axis, whereas the A_g mode indicates the symmetric Sn-S bond stretching in the a-c plane. The spectra are comparable to those of the bulk crystal and concur with past studies on SnS thin films. These results suggest that a SnS thin film with good crystallinity has been synthesized on the glass substrate. Among the Ag modes identified, the peak at 221 cm^{-1} was attributed to the longitudinal optical (LO) mode, while the peak at 94 cm^{-1} was assigned to the transverse optical (TO) mode [2].The films made from bath solutions with high pH values were found to have strong and sharp Raman line intensities, emphasizing good formation in these films.The peak intensities of the SnS thin films increase as the pH of the bath solution increases, which is consistent with the XRD patterns.

Figure 3(b) depicts two distinct bands in the Raman spectra of CdS films at various pH values. These two peaks, which were observed at 300 cm^{-1} and 600 cm^{-1}, respectively, represent the CdS crystal's first and second-order longitudinal optical phonon (LO) modes. The results match those of the bulk crystal and are consistent with earlier studies on CdS thin films[42]. The Raman peak intensities of both films rose as the pH values increased, which is consistent with the XRD patterns.

3.4 Optical Properties

Figures 4(a) & (b) show the absorption spectra (inset) and tau plot of annealed SnS and CdS thin films prepared at different pH values of the source

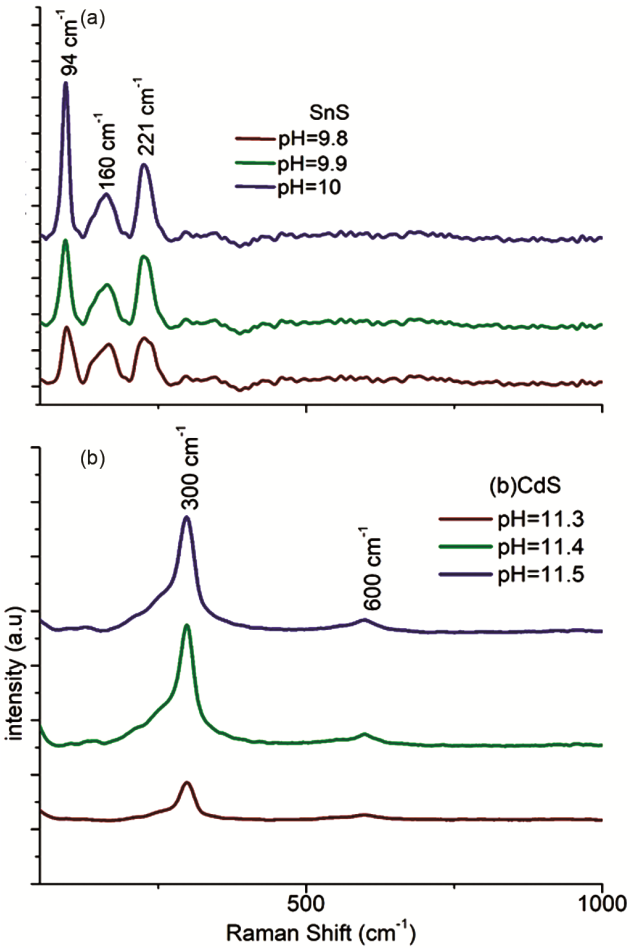

Fig. 3 — Raman analysis of(a) SnSand (b) CdS films deposited with various pH of the bath solution

solutions. The absorption spectra showed a red shift as pH values increased for both SnS and CdS thin films.

The tauc relation connecting bandgap energy and absorption coefficient (α) is given below.

$$\alpha h\upsilon = A\,(h\upsilon - Eg)^{n} \quad \ldots (5)$$

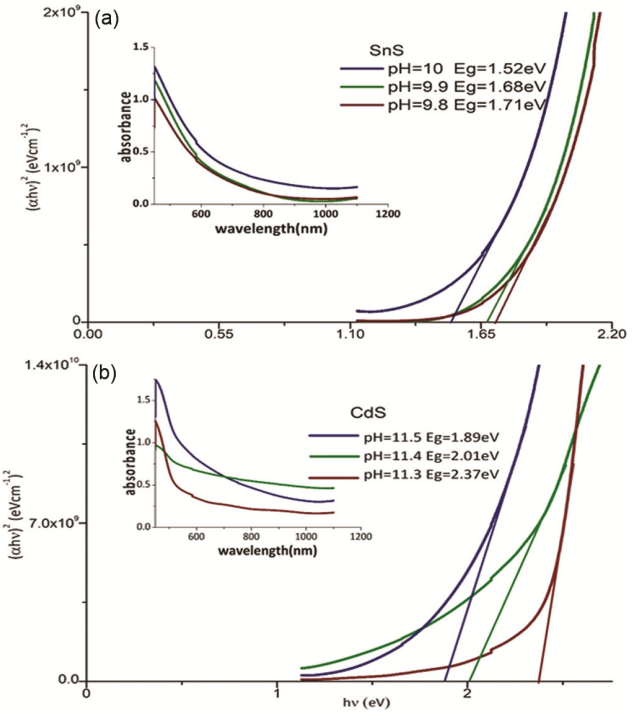

Fig. 4 — Absorption spectra (inset) and Tauc plots of (a) SnS and (b) CdS films deposited with various pH of the bath solution

Where A denotes a constant, h denotes photon energy, υ the frequency, E_g denotes the allowed energy gap, and n = 1/2 denotes the allowed direct transition. For a direct bandgap semiconductor, a tauc plot is drawn with hυ on x the axis and $(\alpha h\upsilon)^2$ on the y axis. The presence of the linear portion in the curve indicates the presence of a direct optical transition in the material. The energy band gap can be determined by extrapolating the straight portion of the plot to the energy axis. The energy gap increases as the pH of the bath solutions decreases for both SnS and CdS. The increase in the energy gap may be due to the existence of grain boundaries in the polycrystalline structures, which results in free carrier concentrations and the existence of potentials in the boundaries. Therefore, an electric field was formed, and the band gap increased. SnS thin films had band gaps of 1.71 eV, 1.68 eV, and 1.52 eV, corresponding to pH values of 9.8, 9.9, and 10, respectively. CdS, on the other hand, had larger band gaps of 2.37 eV, 2.01 eV, and 1.89 eV for pH values of 11.3, 11.4, and 11.5, respectively. Due to its wider optical band gap, CdS can be used as a window layer for the solar cells. Similarly, moderate values of band gap in SnS thin films make them suitable candidates for absorber layers.

3.5 Morphological Studies

Figure 5 displays FESEM images of the SnS and CdS films. While analyzing the morphology of SnS films (Figs. 5(a)–(c)), it was evident that the number of clumps in the film increased and more homogeneous structures formed at higher pH levels. Additionally, it was discovered that the density of clusters gathered at

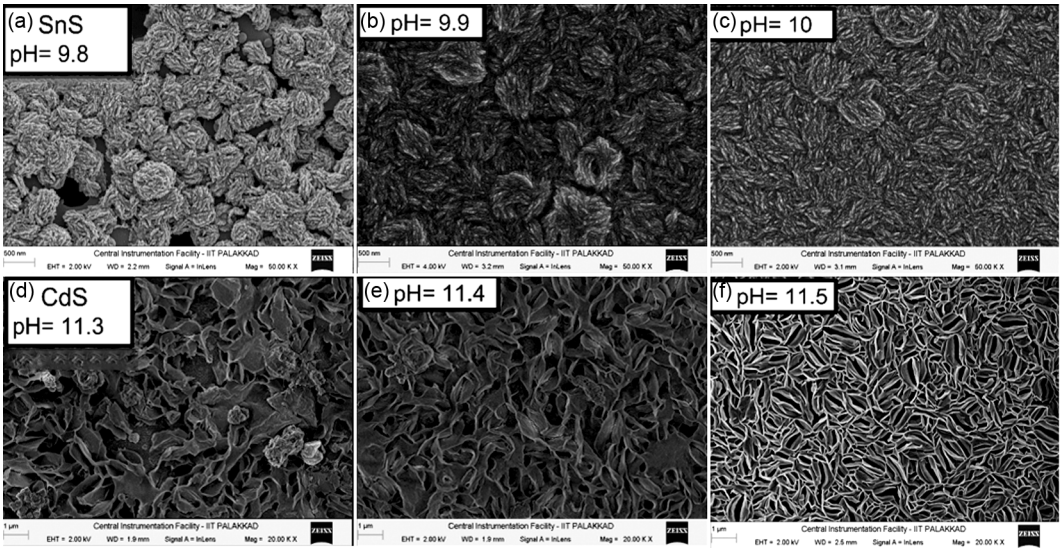

Fig. 5 — Field emission scanning electron microscopy (FESEM) images of (a-c) SnS and (d-f) CdS thin films deposited with various pH of the bath solution

the lowest pH level of 9.8 was low, leaving voids and creating a more porous structure. Fig. 5(d)–(f) depicts the surface morphology of a CdS thin film, which displayed a well-adhered, homogeneous, densely packed, and pinhole-free film. The micrograph also revealed that the films were continuous and had a flake-like morphology. As the pH of the bath solution increased, the interconnected nanoflakes were observed to develop an asymmetrical nanosheet-like morphology and spread throughout the surface.

3.6 Chemical Studies

Figure 6 (a)–(c) indicates the EDS spectra of SnS thin films with various pH values showing the presence of Sn and S peaks. The other unnamed peaks arise from the substrate used. No other contaminant peaks showed up in the spectra. The typical EDS spectra of the CdS thin films for different pH values of bath solution are given in Figure 6 (d)–(f). The cadmium (Cd) and sulphur (S) peaks are clearly visible in the spectra, and other contaminant peaks were absent. The atomic ratios of Sn/S and Cd/S obtained were greater than the expected stoichiometric ratio of unity, which indicates the surface of the sample was rich in metal. Both SnS and CdS thin films go to a metal rich composition with increasing pH values of the bath solution. This finding is consistent with the fact that as the pH of the

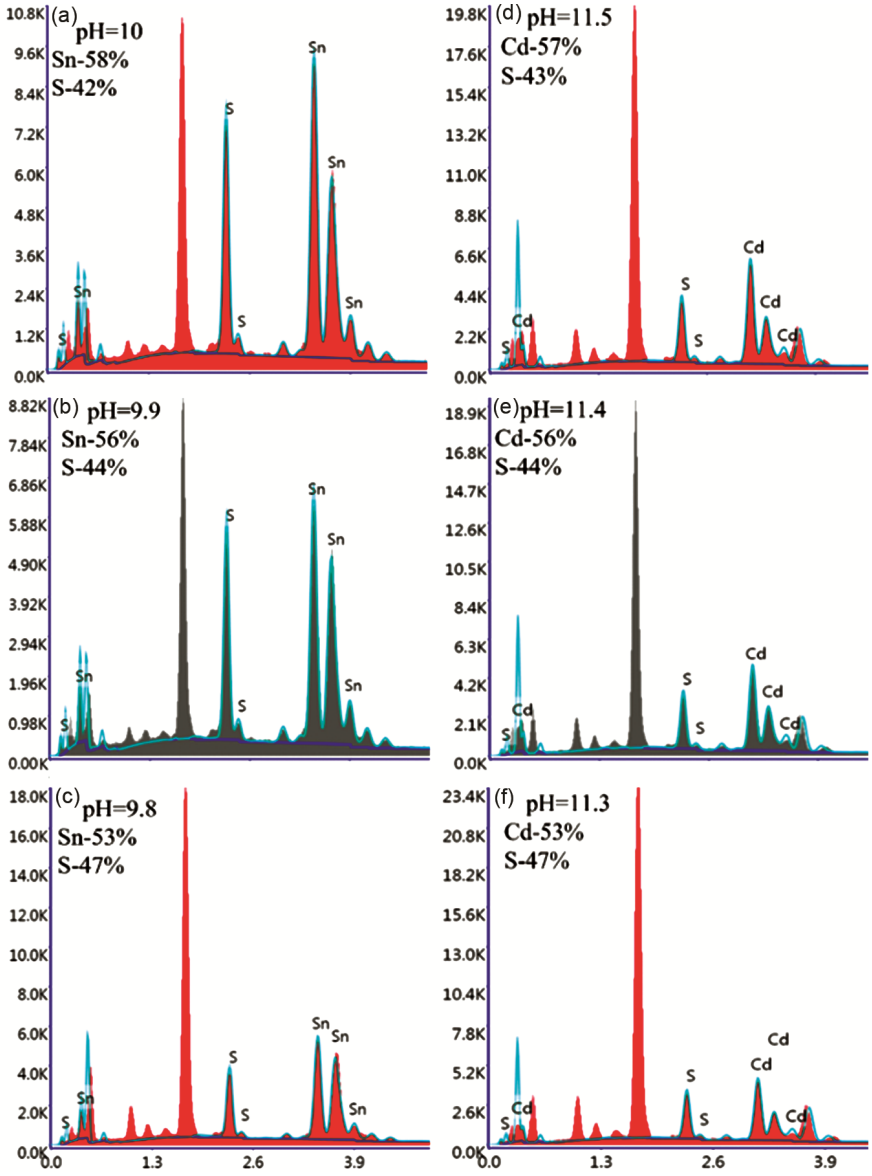

Fig. 6 — EDS images of (a-c) SnS and (d-f) CdS thin films deposited with various pH of the bath solution

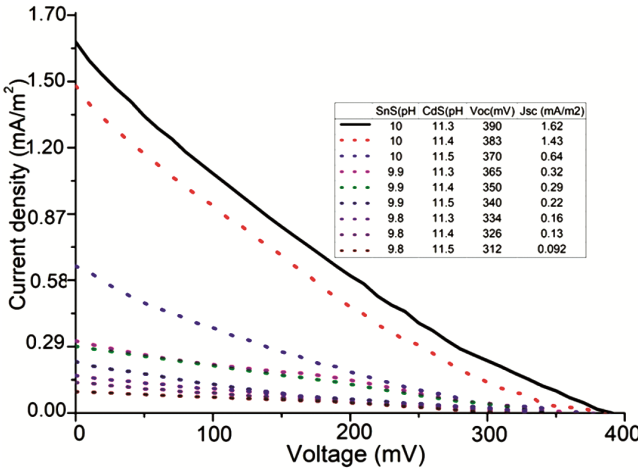

Fig. 7 — I-V characteristics of SnS/CdS photovoltaic cell.

solution increased, the OH-ions liberated more and more cations into the solution.

3.7 I-V Characterization

Finally, a SnS based solar cell was fabricated using commercial ITO (Indium Tin Oxide) as the rear contact, CdS as an n-type semiconductor, SnS as a p-type semiconductor, and silveras the front contact (ITO/SnS/CdS/Ag). I-V characterization for different combinations of pH values is shown in Fig. 7. The table displayed as an inset in the figure shows the open circuit voltage (V_{oc}) and short circuit current (J_{sc}) for all the combinations. Better cell performance was exhibited by the heterojunction fabricated with the combination of SnS with the highest pH value (pH = 10) and CdS with the lowest pH value (pH = 11.3) with a conversion efficiency of 0.12×10^{-3}%.V_{oc}value mainly depend on the crystallinity and the band gap of the absorber layer which is better for the SnS thin films prepared from the bath solution with pH value 10. The value of I_{sc}mainly depends on the density of photons that reaches the junction which is possible when the window layer has wider band gap.In this combination, SnS thin films have the high crystallinity, morphological uniformity, lowest band gap, and high absorption required for an absorber layer, while the CdS film has the highest band gap and lowest absorption, making it suitable for a window layer[4,7,33,43]. Generally, poor photovoltaic efficiency is exhibited by SnS-based solar cells for a number of reasons, including insufficient CBO (Conduction Band Offset), carrier recombination, high resistivity of SnS thin film, sulphur vacancies, low thickness, *etc*.[5,10]. The light trapping techniques like back reflectors and anti-reflective coatings can be used to get a better performance.

4 Conclusions

SnS and CdS thin films were synthesized chemically for different pH values of bath solutions. The optimal pH values for SnS film formation were 9.8, 9.9, and 10, while the pH values for CdS were 11.3, 11.4, and 11.5. Film formation did not take place outside this pH range at ambient conditions. The structural, morphological, optical, and chemical characterization revealed changes in the thin film properties with the pH variation. Structural analysis showed an increase in crystallite size for SnS and CdS as the pH of the solution increased. The optical band gap was found to decrease as the pH of the solution increased for both materials. Morphological studies showed that the film became more continuous and uniform as the pH of the bath solution increased. The atomic weight percentage of metal increased as the pH increased, according to the EDS spectra of both films. Photovoltaic cells were fabricated with an ITO/SnS/CdS/Ag configuration, where the SnS thin film deposited at pH = 10 and the CdS film deposited at pH = 11.3 showed better performance. It was observed that the pH of the bath solution has an effect on the efficiency of the photovoltaic cell. Even though, the cell performance of the fabricated heterojunction was poor, the successful formation of the p-n junction was confirmed. However, SnS thin films are potential candidates for solar cells, and trials can be made to improve the solar cell's performance by optimizing the cell configuration.

Declaration of competing interests

The authors declare that they have no known competing financial interests or personal relationships that could have appeared to influence the work reported in this paper.

Acknowledgements

The authors would like to acknowledge the Department of Science and Technology (DST-FIST), India, for the financial support rendered in setting up the research lab (grant number SR/FST/College-237/2014 (C)) and the University Grants Commission, India, for providing research funds through a minor project (grant number MRP(S)-0191/12–13/KLCA021/UGC-SWRO). The services rendered by SAIF-STIC, CUSAT, and CIF at IIT Palakkad in the form of XRD, SEM, and EDS analysis are also duly acknowledged.

References

1 Patil S B & Singh A K, *Appl Surf Sci*, 256 (2010) 2884.

2 Minnam R V R, Gedi S, Park C, R.w M & Ramakrishna R R, *Curr Appl Phys*, 15 (2015) 588.
3 Cho J Y, Sinha S, Gang M G & Heo J, *J Alloys Compd*, 796 (2019) 160.
4 Cho J Y, Kim S Y, Nandi R, Jang J, Yun H S, Enkhbayar E, Kim J H, Lee D K, Chung C H, Kim J H & Heo J, *J Mater Chem A*, 8 (2020) 20658.
5 Sinsermsuksakul P, Sun L, Lee S W, Park H H, Kim S B, Yang C & Gordon R G, *Adv Energy Mater*, 4 (2014) 1.
6 Loferski J J, *J Appl Phys*, 27 (1956) 777.
7 Kuddus A, Mostaque S K & Hossain J, *Opt Mater Express*, 11 (2021) 3812.
8 Chalapathi U, Poornaprakash B, Choi W J & Park S H, *Appl Phys A Mater Sci Process*, 126 (2020) 1.
9 Vidal J, Lany S, D'Avezac M, Zunger A, Zakutayev A, Francis J & Tate *J, Appl Phys Lett*, 100 (2012).
10 Andrade-Arvizu J A, Courel-Piedrahita M & Vigil-Galán O, *J Mater Sci Mater Electron*, 26 (2015) 4541.
11 Boubakri A, Jouidri A, Koumya Y, Rajira A, Almaggoussi A & Abounadi A, *Mater Today Proc*, 51 (2021) 2047.
12 Sattarian H, Tohidi T & Rahmatallahpur S, *Mater Sci Pol*, 34 (2016) 540.
13 Khot K V., Mali S S, Kharade R R, Mane R M, Patil P S, Hong C K, Kim J H, Heo J, & Bhosale P N, *J Mater Sci Mater Electron*, 25 (2014) 5606.
14 Singh B, Singh J, Kaur J, Moudgil R K & Tripathi S K, *Phys B Condens Matter*, 490 (2016) 49.
15 Ganchev M, Vitanov P, Sendova-Vassileva M, Popkirov G & Dikov H, *J Phys Conf Ser*, 682 (2016).
16 Hartman K, Johnson J L, Bertoni M I, Recht D, Aziz M J, Scarpulla M A & Buonassisi T, *Thin Solid Films*, 519 (2011) 7421.
17 Moon B S, Lee J H & Jung H, *Thin Solid Films*, 511 (2006) 299.
18 Mlowe S, Lewis D J, Azad Malik M, Raftery J, Mubofu E B, O'Brien P & Revaprasadu N, *New J Chem*, 38 (2014) 6073.
19 Ahmet I Y, Hill M S, Johnson A L & Peter L M, *Chem Mater*, 27 (2015) 7680.
20 Altiokka B & Yildirim A K, *J Korean Phys Soc*, 72 (2018) 687.
21 Mariappan R, Mahalingam T & Ponnuswamy V, *Optik (Stuttg)*, 122 (2011) 2216.
22 Johny J, Sepulveda-Guzman S, Krishnan B, Avellaneda D A, Aguilar Martinez J A & Shaji S, *Chem Phys Chem*, 18 (2017) 1061.
23 Orlianges J C, Champeaux C, Dutheil P, Catherinot A & Mejean T M, *Thin Solid Films*, 519 (2011) 7611.
24 Santhosh K K, Manoharan C, Dhanapandian S & Gowri M A, *Spectrochim Acta - Part A Mol Biomol Spectrosc*, 115 (2013) 840.
25 Aboud A A, Mukherjee A, Revaprasadu N & Mohamed A N, *J Mater Res Technol*, 8 (2019) 2021.
26 Desale D J, Shaikh S, Siddiqui F, Ghosh A, Birajdar R, Ghule A & Sharma R, *Adv Appl Sci Res*, 2 (2011) 417.
27 Ghosh B, Das M, Banerjee P & Das S, *Appl Surf Sci*, 254 (2008) 6436.
28 Sattarian H, Tohidi T & Rahmatallahpur S, *Mater Sci Pol*, 34 (2016) 540.
29 Su M S, Kuo C Y, Yuan M C, Jeng U S, Su C J & Wei K H, *Adv Mater*, 23 (2011) 3315.
30 Kabiri S N, Dehghani T Z, Bioki H A, Zarandi M B & Shayegh S, *Optik (Stuttg)*, 131 (2017) 231.
31 Yue G H, Wang W, Wang L S, Wang X, Yan P X, Chen Y & Peng D L, *J Alloys Compd*, 474 (2009) 445.
32 Mishra S, Ingale A, Roy U N & Gupta A,*Thin Solid Films*, 516 (2007) 91.
33 Chalapathi U, Poornaprakash B & Park S H, *Sol Energy*, 139 (2016) 238.
34 Jing J, Cao M, Wu C, Huang J, Lai J, Sun Y, Wang L & Shen Y, *J Alloys Compd*, 726 (2017) 720.
35 Raut V S, Lokhande C D & Killedar V V, *Int J Eng Res Technol*, 10 (2017) 568.
36 Ben N T, Kamoun N, Kanzari M & Bennaceur R, *Thin Solid Films*, 500 (2006) 4.
37 Maghouli M & Eshghi H, *Superlattices Microstruct*, 128 (2019) 327.
38 Higareda-Sánchez A, Mis-Fernández R, Rimmaudo I, Camacho-Espinosa E & Peña J L, S*uperlattices Microstruct*, 151 (2021).
39 Guneri E, Gode F, Ulutas C, Kirmizigul F, Altindemir G & Gumus C, *Chalcogenide Lett*, 7 (2010) 685.
40 Andrade A B, Ferreira N S & Valerio M E G, *RSC Adv*, 7 (2017) 26839.
41 Shaaban E R, Afify N & El-Taher A, *J Alloys Compd*, 482 (2009) 400.
42 Gilic M, Trajic J, Romcevic N, Romcevic M, Timotijevic D V, Stanisic G & Yahia I S, *Opt Mater (Amst)*, 35 (2013) 1112.
43 Minbashi M, Ghobadi A, Ehsani M H, Rezagholipour D H & Memarian N, *Sol Energy*, 176 (2018) 520.